

RESEARCH ARTICLE

10.1002/2017MS001157

Special Section:

The Energy Exascale Earth System Model (E3SM)

Key Points:

- Convective gustiness is shown to reduce the low precipitation bias in the Tropical West Pacific during Boreal summer
- Convective gustiness increases precipitation in regions where resolved winds are weak and convective precipitation is strong
- Increases in surface evaporation invigorate the circulation, increasing divergence of moist static energy out of the Tropical West Pacific

Correspondence to:

B. E. Harrop,
bryce.harrop@pnnl.gov

Citation:

Harrop, B. E., Ma, P.-L., Rasch, P. J., Neale, R. B., & Hannay, C. (2018). The role of convective gustiness in reducing seasonal precipitation biases in the Tropical West Pacific. *Journal of Advances in Modeling Earth Systems*, 10, 961–970. <https://doi.org/10.1002/2017MS001157>

Received 6 SEP 2017

Accepted 7 MAR 2018

Accepted article online 12 MAR 2018

Published online 10 APR 2018

© 2018. The Authors.

This manuscript has been authored by Battelle Memorial Institute under contract DE-AC05-76RL01830 with the U.S. Department of Energy. The United States Government retains and the publisher, by accepting the article for publication, acknowledges that the United States Government retains a nonexclusive, paid-up, irrevocable, worldwide license to publish or reproduce the published form of this manuscript, or allow others to do so, for United States Government purposes.

This is an open access article under the terms of the Creative Commons Attribution-NonCommercial-NoDerivs License, which permits use and distribution in any medium, provided the original work is properly cited, the use is non-commercial and no modifications or adaptations are made.

The Role of Convective Gustiness in Reducing Seasonal Precipitation Biases in the Tropical West Pacific

Bryce E. Harrop¹, Po-Lun Ma¹, Philip J. Rasch¹, Richard B. Neale², and Cecile Hannay²

¹Atmospheric Sciences and Global Change Division, Pacific Northwest National Laboratory, Richland, Washington, USA,

²National Center for Atmospheric Research, Boulder, Colorado, USA

Abstract Precipitation is an important climate quantity that is critically relevant to society. In spite of intense efforts, significant precipitation biases remain in most climate models. One pervasive and persistent bias found in many general circulation models occurs in the Tropical West Pacific where northern hemisphere summer-time precipitation is often underestimated compared to observations. Using the DOE-E3SM model, the inclusion of a missing process, convective gustiness, is shown to reduce those biases through a net increase in surface evaporation. Gustiness in surface wind fields is assumed to arise empirically in proportion to the intensity of convective precipitation. The increased evaporation can be treated as an increase in the moist static energy forcing into the atmosphere. A Normalized Gross Moist Stability (NGMS) framework (which characterizes the relationship between convective forcing and convective response) is used to explore the processes responsible for the precipitation bias, and the impact of the gustiness parameterization in reducing that bias. Because the NGMS of the Tropical West Pacific is less than unity in the E3SMv1 model, the increase in energy forcing amplifies the increase in precipitation to exceed that of the evaporative flux. Convective gustiness favors increased precipitation in regions where the resolved surface winds are weak and convection is present.

Plain Language Summary The Tropical West Pacific is a region of very strong rainfall and weak surface winds. Climate models often underestimate rainfall in the Tropical West Pacific during the summer. The shortage of rain is related to the low amount of evaporation arising from the light surface winds in the region. General circulation models have typically neglected gusts that are generated below evaporating rain, but these gusts are known to create circulations that increase surface evaporation. Accounting for these “gusty winds” increases surface evaporation in the model, which acts as a local source of moist energy to the atmosphere, intensifying the circulation and surface rainfall amount. Including gustiness leads to a more realistic rainfall pattern when compared to the real world.

1. Introduction

Rainfall reaching the surface is one of the most human-relevant components of the climate system. Accurate modeling of precipitation in the current climate is a necessary step in understanding and projecting how precipitation will change in a CO₂-warmed world. There remain, however, deficiencies in climate models in the prediction of precipitation even in the current climate. Sperber et al. (2013) showed that model precipitation biases in the Asian monsoon region have been particularly difficult to improve, with both the CMIP3 and CMIP5 multimodel mean precipitation distributions being nearly identical across much of the Tropical West Pacific and Indian Oceans.

Surface fluxes of sensible and latent heat have been shown to be sensitive to parameterization choices in low wind conditions (Miller et al., 1992; Webster & Lukas, 1992; Zeng et al., 2002). One such low wind region is just north of the maritime continent—which we refer to as the northern Tropical West Pacific (TWP). Brunke et al. (2008) showed a strong sensitivity of the northern TWP precipitation to a skin temperature parameterization in the Community Atmosphere Model version 3.1 (CAM3.1; Collins et al., 2006). They showed that they could remediate much of a negative precipitation bias in the northern TWP in CAM3.1 through a modification to the ocean skin temperature parameterization that increased the surface latent heat flux in that region. The CAM5 model (Neale et al., 2012) and the Energy Exascale Earth System Model

(E3SM) versions 0 and 1 all have similar precipitation biases in the northern TWP to CAM3.1, though we focus only on the E3SMv1 model in this manuscript.

In this work, we show that the inclusion of convective gustiness, a model parameterization designed to capture the increased surface evaporation in the presence of unresolved convective downdrafts, also reduces the northern TWP precipitation bias. Making use of a Normalized Gross Moist Stability (NGMS) framework (see, for example, Raymond et al., 2007, 2009), we identify the regions in the model where precipitation is most susceptible to surface evaporation increases. The NGMS diagnostic indicates that an increase in evaporation (from gustiness) amplifies precipitation in the northern TWP region. NGMS also provides a framework to understand the required response of the atmospheric circulation to convective gustiness. We further discuss the response of the circulation to gustiness in terms of its seasonal progression, represented as a monsoon circulation over the northern TWP region. An outline of the work presented in this manuscript is as follows: in section 2, we document the data and methods used; in section 3, we provide the results of our analyses (broken into the precipitation response, circulation response, and monsoon response), as well as discussion thereof; and in section 4, we provide conclusions and final remarks.

2. Methods and Data

We use the Energy Exascale Earth System Model (E3SM) version 1 atmosphere model with a fixed monthly varying climatological sea surface temperature (SST). All the inputs and boundary conditions (such as SSTs, well-mixed greenhouse gases, and aerosol emissions) are representative of the year 2000. The model uses a spectral element dynamical core with a horizontal grid spacing approximately equal to 1 degree. The model employs the CLUBB higher order turbulence parameterization (Golaz et al., 2002a, 2002b; Larson et al., 2002; Larson & Golaz, 2005) to unify the treatment of cloud macrophysics, turbulence, and shallow convection using probability distribution functions that describes the subgrid variability of model fields. CLUBB therefore produces precipitation events associated with shallow convection, and resolved and unresolved stratiform clouds. The Zhang-McFarlane parameterization (Neale et al., 2008; Zhang & McFarlane, 1995) is used to represent a subgrid scale spectrum of deep convective cloud types. Both the control and experimental simulations are run for 6 years, discarding the first year as spin-up.

A new parameterization is introduced to represent increased surface wind speeds often observed in the presence of cold pools associated with evaporating rainfall in deep convection downdrafts. The surface wind speed used in the surface heat flux calculations (sensible and latent) is increased in proportion to the intensity of convective precipitation reaching the surface. The parameterization follows Redelsperger et al. (2000) by adding a nonlinear term to the wind speed used in the surface evaporation computation:

$$\begin{aligned} \bar{U}^2 &= U_0^2 + U_g^2 \\ U_0 &= \|\bar{\mathbf{U}}\| \\ U_g &= \begin{cases} \log(1.0 + 6.69R - 0.476R^2), & R < 6 \text{ cm/d} \\ 3.2 \text{ m/s}, & R \geq 6 \text{ cm/d} \end{cases} \end{aligned} \quad (1)$$

Here U_0 is the resolved surface wind speed, U_g is the wind speed enhancement owing to convective gustiness, and R is the convective rain rate at the surface. The parameterization of Redelsperger et al. (2000) for convective gustiness is based on CRM modeling of TOGA COARE (Webster & Lukas, 1992) data. There is a saturation of gustiness winds around 3 m/s occurring for rain rates above 6 cm/d, as noted in equation (1). The parameterization only accounts for increases in wind speed, not the increase in sensible heat flux owing to colder air within cold pools (the latter effect was shown to be secondary to the enhanced wind speed by Jabouille et al. (1996). Likewise, drier air mixed into the boundary layer by downdrafts is also not a source of enhanced surface evaporation. Redelsperger et al. (2000) also developed parameterizations based on upward and downward convective mass flux, as well as a formulation for boundary layer convection. We select the parameterization based on convective rain rate for simplicity, and opt to leave the boundary layer formulation for future investigations because we expect deep convection to be more important in the northern TWP region that we focus on. Gustiness is very important in the tropics where deep convective precipitation dominates the total surface precipitation flux (see Figure 1).

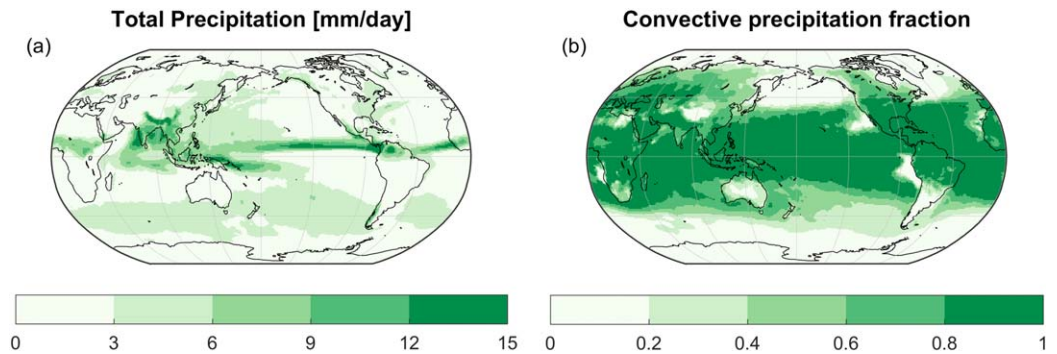


Figure 1. (a) Total JJA surface rain rate (mm/d) in the control experiment and (b) fraction of JJA surface precipitation owing to convection in the control experiment.

In this study, convective gustiness is only applied over ocean surfaces in the model. Over land, it is unclear whether the complex surface can be well approximated by the Redelsperger et al. (2000) parameterization. Vegetated surfaces, for example, may require a different parameterization to properly account for the enhanced fluxes beneath convection. For model grid spaces that include a mix of land and ocean, there are two separate surface flux calculations, and only those over ocean receive the enhancement owing to convective gustiness.

We run two simulations: one without convective gustiness (control) and one with convective gustiness (gusty). Because the precipitation bias in the northern TWP is dominated by errors during the northern hemisphere summer, we restrict all of our analyses to the JJA season.

Figure 2a shows the mean JJA precipitation pattern bias of the control simulation compared with the CPC Merged Analysis of Precipitation (CMAP) observationally based estimate (Xie & Arkin, 1996, 1997). The bias pattern is similar when compared with other precipitation data sets such as the Global Precipitation Climatology Project (Adler et al., 2003) though the magnitude differs (not shown). There is a clear underestimate of JJA precipitation in the northern TWP region. The tropical rain belt remains fixed over the maritime continent during JJA in the control simulation, while it migrates to the north in observations.

Plots b and c of Figure 2 show both evaporation and precipitation increase owing to convective gustiness in the northern TWP region. The increase in evaporation is unsurprising given the formulation of the

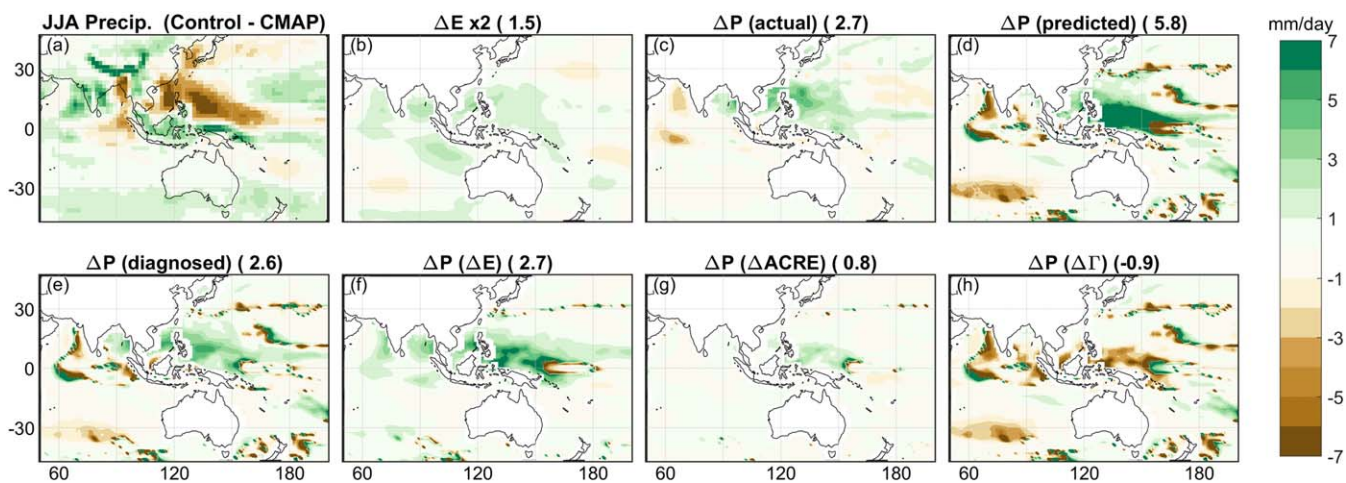


Figure 2. (a) Precipitation bias between control simulation and CMAP observations; (b) change in evaporation owing to convective gustiness ($E_{gust} - E_{ctrl}$ multiplied by a factor of 2); (c) change in precipitation owing to convective gustiness ($P_{gust} - P_{ctrl}$); (d) predicted change in precipitation owing to convective gustiness following equation (11); (e) diagnosed precipitation change following equation (6); (f) contribution of precipitation change coming from changes in evaporation ($E_{ctrl}((1 + (U_g/U_0)^2)^{1/2})(1 + (1/\Gamma_{ctrl})))$); (g) contribution of precipitation change coming from changes in ACRE ($\Delta ACRE/L\Gamma_{ctrl}$); and (h) contribution of precipitation change coming from changes in NGMS ($(\nabla \cdot [vq])_{ctrl}(\Delta\Gamma/\Gamma_{ctrl})$). The storage terms in Figures 2d and 2e are negligible and not shown here. In each plot, “ Δ ” refers to the difference between gustiness and the control. All plots are given in mm/d for JJA.

convective gustiness in equation (1), and we argue that this increase in evaporation is the main cause of the increased precipitation, despite the increase in precipitation exceeding that of evaporation. Figure 2 (plots a and c) is comparable to Figure 9 (plots b and c) of Brunke et al. (2008), which used a different parameterization change to influence this precipitation feature. The dry bias to the west of the Indochinese Peninsula is improved, while there is little change just west of Sumatra. The precipitation increase over the Bay of Bengal likely results from the precipitation moving northward and the feedback of that precipitation enhancing evaporation to invigorate even more precipitation. It is unclear why there is little change in the Indian Ocean just west of Sumatra. It may be that this bias is not the result of underrepresented surface evaporation, but some other physical process.

It is important to note that we do not include the skin temperature parameterization used in Brunke et al. (2008) here. It would be useful to know how precipitation responds to both parameterizations, as well as quantify the importance of both, but we leave these questions for future work. Both Brunke et al. (2008) and Miller et al. (1992) found similar precipitation responses to increases in evaporation in the northern TWP, but did not offer a physical explanation for the underlying mechanism linking the increases in evaporation and precipitation. Here we aim to understand that physical mechanism. Because the gustiness evaporation enhancement is formulated to be a function of convective precipitation, we expect strong feedbacks to occur between precipitation and evaporation. We do not aim to describe and predict the full scope of those feedbacks, but instead seek the physical mechanism responsible for initiating the feedback process.

We have chosen to evaluate the model deficiencies, and mechanisms for its improvement by employing the NGMS diagnostic framework of Raymond et al. (2009). NGMS is defined as the ratio of column-integrated MSE divergence to column-integrated latent energy divergence, which can be related to energy forcing, evaporation, and precipitation through the energy and moisture budget equations

$$\Gamma \equiv -\frac{\nabla \cdot [\mathbf{v}h]}{L\nabla \cdot [\mathbf{v}q]} = -\frac{F_S - R - \frac{\partial[h]}{\partial t}}{LE - LP - L\frac{\partial[q]}{\partial t}} \quad (2)$$

Here Γ is the NGMS, \mathbf{v} is the 2-D velocity, h is the moist static energy (MSE), q is the specific humidity, L is the latent heat of vaporization, square brackets denote the total column integral, F_S is the surface energy forcing (sensible plus latent heat flux), R is the radiative cooling, P is the precipitation, and E is the evaporation. NGMS is of interest here because it measures the relative importance of forcing changes to responses in the moisture cycle. For example, if NGMS is positive and less than one, then an increase in forcing will drive an even larger change in P-E (when measured in the same units) assuming that NGMS remains roughly constant. The NGMS framework allows us to think of an increase in evaporation as an increase in MSE forcing which can drive increases in precipitation exceeding the changes in evaporation.

Equation (2) can be rewritten to express precipitation as a function of the other terms in (2)

$$LP = LE - L\frac{\partial[q]}{\partial t} + \frac{F_S - R - \frac{\partial[h]}{\partial t}}{\Gamma} \quad (3)$$

Equation (3) can be used to derive an expression for ΔP assuming that the change in total energy forcing is equivalent to the change in evaporative flux and Atmospheric Cloud Radiative Effect (i.e., $\Delta(F_S - R) \approx L\Delta E + \Delta \text{ACRE}$, which is shown to be a reasonable assumption for these experiments in Figure 3) as:

$$L\Delta P \approx L\Delta E - \Delta\left(L\frac{\partial[q]}{\partial t}\right) + \frac{L\Delta E + \Delta \text{ACRE}}{\Gamma_{ctrl}} - \left(F_S - R - \frac{\partial[h]}{\partial t}\right)_{ctrl} \frac{\Delta\Gamma}{\Gamma_{ctrl}^2} - \frac{1}{\Gamma_{ctrl}} \Delta\left(\frac{\partial[h]}{\partial t}\right) \quad (4)$$

In the northern TWP region, the change in energy flux ($\Delta(F_S - R) = 28.7 \text{ W/m}^2$) is balanced 75% by $L\Delta E$ (21.5 W/m^2) and 29% by ΔACRE (8.2 W/m^2), with a residual of -1.1 W/m^2 . Taking advantage of the definition of NGMS in equation (2) as:

$$L\Delta P \approx L\Delta E \left(1 + \frac{1}{\Gamma_{ctrl}}\right) + \frac{\Delta \text{ACRE}}{\Gamma_{ctrl}} - \Delta\left(L\frac{\partial[q]}{\partial t}\right) + (L\nabla \cdot [\mathbf{v}q])_{ctrl} \left(\frac{\Delta\Gamma}{\Gamma_{ctrl}}\right) - \frac{1}{\Gamma_{ctrl}} \Delta\left(\frac{\partial[h]}{\partial t}\right) \quad (5)$$

The storage terms (the third and fifth terms on the RHS of equation (5)) are negligible compared to the other terms in equation (5) (negligible here means more than an order of magnitude smaller). Dropping these storage terms gives the following equation for ΔP :

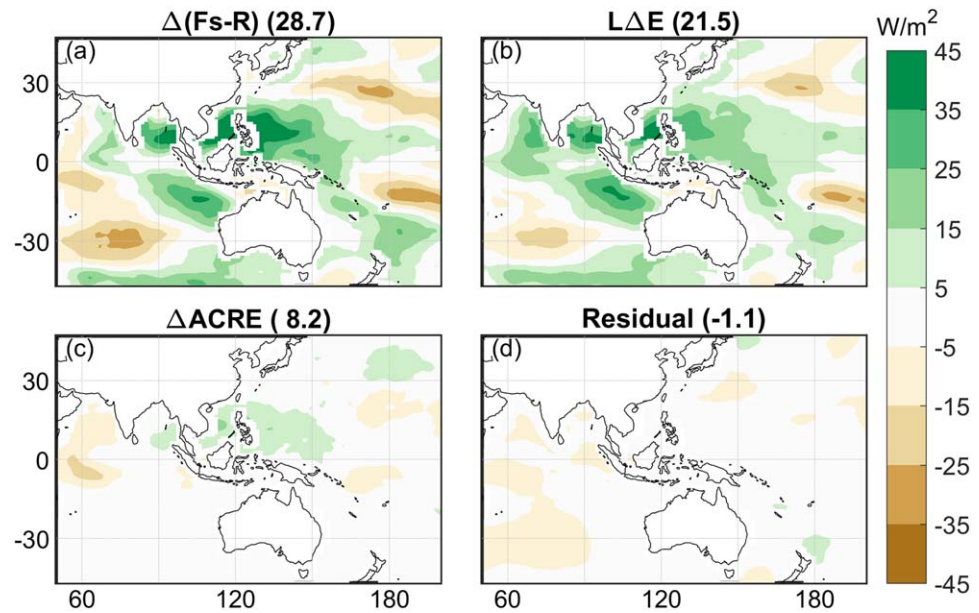


Figure 3. Difference in (a) net energy forcing, (b) surface latent heat flux, (c) ACRE, and (d) residual between the gustiness and control experiments. The values in the subtitles are the average for the northern TWP region (110–150E, 5–25N). All values are for JJA.

$$\Delta P \approx \Delta E \left(1 + \frac{1}{\Gamma_{ctrl}} \right) + \frac{\Delta ACRE}{L\Gamma_{ctrl}} + (\nabla \cdot [\mathbf{v}q])_{ctrl} \left(\frac{\Delta \Gamma}{\Gamma_{ctrl}} \right) \quad (6)$$

The latent heat of vaporization term is dropped in equation (6) for convenience since ΔP takes the same units as ΔE and $\nabla \cdot [\mathbf{v}q]$. Equation (6) provides an expression for diagnosing the change in precipitation between the control and gusty experiments. The first term on the RHS of equation (6) is directly related to the change in evaporation, which is precisely how convective gustiness operates on the model climate and a term that we can predict using the gustiness formulation. Therefore, we next seek to frame ΔE in terms of the gustiness formulation from equation (1). The bulk aerodynamic formulae for the two evaporative fluxes (with and without gustiness) are:

$$E_{ctrl} = \rho C_{DE} (U_0^2)^{1/2} (q_s - q_a) \quad (7)$$

$$E_{gsty} = \rho C_{DE} (U_0^2 + U_g^2)^{1/2} (q_s - q_a) \quad (8)$$

Since ρ , C_{DE} , and $(q_s - q_a)$ are the same in both equations, the predicted change in evaporation must come from including the gustiness wind speed, U_g . In reality, the model uses Monin-Obukhov similarity theory to predict the surface exchange of momentum, sensible heat, and latent heat fluxes. The bulk aerodynamic formulae serve as a simple conceptual model for understanding the impact changing the surface winds through convective gustiness has on the evaporation, as well as the subsequent changes in precipitation. Additionally, the drag coefficient, C_{DE} , is not constant within the model, but depends on wind speed. Offline calculations suggest gustiness in the northern TWP may reduce the drag coefficient by roughly 20%. We discuss the ramifications of this simplified model for predicting precipitation changes in section 3a. Thus, within this simplified framework, the evaporation owing to gustiness may be written as a function of evaporation from the control experiment and the ratio of gusty to resolved wind speeds.

$$E_{gsty} = E_{ctrl} \left(\frac{U_0^2 + U_g^2}{U_0^2} \right)^{1/2} = E_{ctrl} \left(1 + (U_g/U_0)^2 \right)^{1/2} \quad (9)$$

$$\Delta E = E_{ctrl} \left(\sqrt{1 + (U_g/U_0)^2} - 1 \right) \quad (10)$$

Finally, combining equations (6) and (10) gives a prediction for the response of precipitation to convective gustiness:

$$\Delta P \approx E_{ctrl} \left(\sqrt{1 + (U_g/U_0)^2} - 1 \right) \left(1 + \frac{1}{\Gamma_{ctrl}} \right) + \frac{\Delta ACRE}{L\Gamma_{ctrl}} + (\nabla \cdot [\mathbf{v}q])_{ctrl} \left(\frac{\Delta \Gamma}{\Gamma_{ctrl}} \right) \quad (11)$$

We use equation (11) to diagnose the expected changes in precipitation owing to convective gustiness in the next section.

3. Results and Discussion

3.1. Precipitation Response

Plots b and c of Figure 2 show the evaporation and precipitation responses, respectively, owing to convective gustiness. Because we do not include gustiness over land in these simulations, we have masked out any grid cells containing land in Figure 2 (except in plot a). Plots d and e of Figure 2 show the precipitation change owing to convective gustiness predicted and diagnosed from equations (11) and (6), respectively. For the prediction of ΔP , we use the 6 hourly output to compute the gustiness enhancement to evaporation and compute the first term of equation (11) that way. For the diagnosed ΔP values in plot e, we take the actual ΔE field shown in plot b (without the multiplication factor). Figure 2d shows the predicted change in precipitation computed using equation (11). Comparing plots c and d of Figure 2, we see an increase in precipitation over the northern TWP region (110–150E, 5–25N) for both the actual change in precipitation owing to convective gustiness and that predicted by equation (11). The same increase in precipitation owing to convective gustiness is also diagnosed well by equation (6) (Figure 2e). To gain further physical insight, the diagnosed precipitation change is separated into the three terms in equation (6). Figure 2, plots f, g, and h, shows the diagnosed precipitation changes owing to evaporation, ACRE, and NGMS. It is clear from comparing plots f, g, and h that precipitation in the northern TWP region increases owing exclusively to the evaporation (ΔE) and ACRE ($\Delta ACRE$) terms. The change in NGMS between the two experiments actually suggests precipitation should decrease in the northern TWP (Figure 2h). In the control simulation, NGMS is positive in areas of active convection (Figure 4) because there is divergence of moist static energy collocated with convergence of moisture. Since Γ is positive and $\nabla \cdot [\mathbf{v}q]$ is negative, the decrease in precipitation in Figure 2h implies an increase in NGMS in the northern TWP, and indeed NGMS does increase slightly when convective gustiness is included in the model (not shown). The decrease in precipitation related to the increasing NGMS (Figure 2h) is largely offset by the increase in precipitation related to the increase in ACRE (Figure 2g). Both of these terms, however, are still much smaller in magnitude than the term related to surface evaporation changes.

Predicted ΔP (Figure 2d) is approximately twice as large as the actual (Figure 2c) and diagnosed (Figure 2e) ΔP for the northern TWP region. Likewise, the surface evaporative flux is roughly twice as large when computed using the gustiness ΔE in equation (10) compared to the actual change in ΔE in the northern TWP. This difference in surface evaporation is likely a shortcoming of our simplified model for surface evaporation

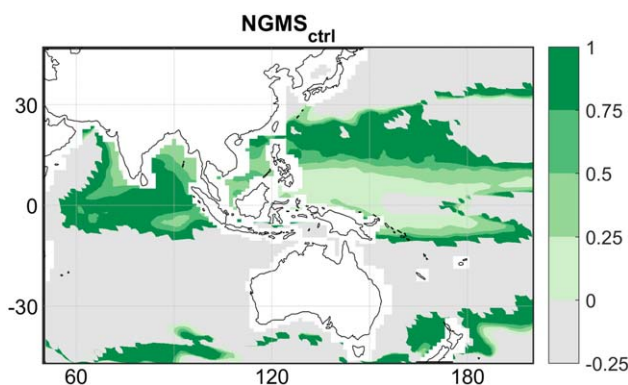


Figure 4. Normalized Gross Moist Stability (unitless) for JJA in the control simulation. Note that negative values of NGMS are possible, though we ignore them here since they tend to occur outside of the deep convective zones of the tropics.

(using the bulk aerodynamic formulae in place of the Monin-Obukhov similarity set of equations). Despite this limitation, the predicted ΔP still identifies the importance of convective gustiness in driving increases in precipitation in the northern TWP, verifying that this simple model is capable of predicting the regions that are sensitive to gustiness. As mentioned above, the predicted change in precipitation may be sensitive to the drag coefficient, C_{DE} , which was assumed constant in equation (11), but actually varies as a function of wind speed. Taking into account variations in C_{DE} changes the predicted precipitation amount over the northern TWP from 5.8 to 4.8 mm/d, which is still substantially larger than the actual value of 2.7 mm/d, but does not change the spatial pattern of precipitation increase (not shown). The predicted precipitation metric shows that while the magnitude of precipitation change is sensitive to the total adjustment of the atmosphere, the regions that are sensitive to surface wind speed changes (through processes such as convective gustiness) can be identified with the simple framework represented by equation (11).

Since the first term in the RHS of equation (11) dominates the total response (compare Figure 2f with Figures 2g and 2h), the change in precipitation owing to gustiness must come from either the change in evaporation, the pattern of NGMS, or some combination of the two. To test whether the pattern of NGMS is important, the change in precipitation is recalculated using a fixed NGMS (≈ 0.4 , equal to the average value over the convective zones of the tropics—defined as those regions between 20S and 20N where total precipitation exceeds 2 mm/d). The difference in ΔP diagnosed using this fixed value of NGMS compared to that using the true spatial distribution of NGMS is negligible (less than 0.05 mm/d over the northern TWP; not shown). Thus, it must be the evaporation change—which primarily results from gustiness—that accounts for the pattern change in precipitation predicted in Figure 2d. It is important to note that the increase in precipitation owing to evaporation changes diagnosed in Figure 2f is much larger than the actual evaporation changes in Figure 2b, implying most of the water supplying the increased precipitation comes from increased moisture convergence, not local surface evaporation. In this sense, it is best to think of the increased surface evaporation as an MSE source that enhances the circulation and increases precipitation that way.

As can be seen by equation (6), the increase in precipitation owing to increased evaporation is modulated by the NGMS. The northern TWP is a region where NGMS is between zero and one, meaning that the divergence of MSE is smaller than the convergence of latent energy (LE). Increasing evaporation, and hence latent heat flux, requires an increase in either (or both) local radiative cooling or divergence of MSE. Since the radiative heating actually increases (owing to the increase in ACRE), the divergence of MSE must be increasing. Under constant NGMS conditions, any increase in divergence of MSE must be met with a proportionally larger increase in LE convergence. If we assume that the divergence of MSE is equal to the increased evaporation by gustiness, then we can expect the increase in precipitation to exceed the increase in evaporation, which it does—evaporation increases by 22 W/m² (20%) and precipitation by 77 W/m² (49%) over the northern TWP. As we noted above, the increase in ACRE also contributes to the increase in precipitation, but it is largely offset by increased NGMS which reduces the moisture convergence relative to MSE divergence. Mathematically, this is obvious from the first term in the RHS of equation (6), but it is useful to consider what it means physically. Instead of treating surface evaporation simply as a moisture source, treating it as an energy source allows us to correctly diagnose the increase in precipitation owing to convective gustiness in the model. As a source of MSE, the increase in surface evaporation requires an intensification of the circulation to diverge more MSE. As can be seen in Figure 5, the increase in MSE divergence occurs in the upper troposphere, with increased convergence at low levels, implying enhanced vertical motion, which gives rise to the increase in precipitation seen between the two simulations.

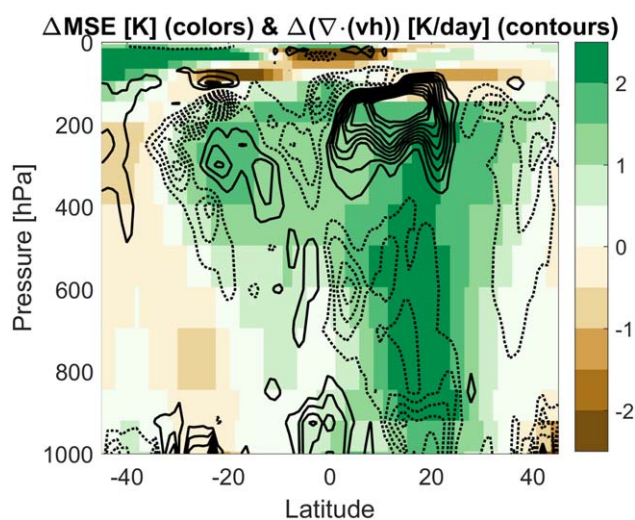


Figure 5. Change in MSE (colors) and divergence of MSE flux (contours) owing to convective gustiness for JJA. Both h and $\nabla \cdot (vh)$ are scaled by $(1/C_p)$, where C_p is the specific heat of dry air at constant pressure, such that Δh is given in units of K and $\Delta(\nabla \cdot (vh))$ is given in units of K/d. All values are zonally averaged over 110–150E.

Equation (10) suggests the largest increase in evaporation comes from regions where the wind enhancement owing to convective gustiness (U_g/U_0) is large. Figure 6a shows that the regions of low wind speed are collocated with those predicted to show the largest increases in precipitation (Figure 2c). Figure 6b shows these same regions are where the gustiness wind speeds (U_g) exceed those of the resolved circulation (U_0). The northern TWP is one such region. It is clear that convective gustiness produces precipitation enhancement in regions where the climatological resolved wind speed is low and where convection occurs. Earlier work (e.g., Zeng et al., 2002) has shown evaporation to be sensitive to low wind conditions. Since our analysis above has shown the changes in precipitation are dominated by evaporation changes, then it is clear that the sensitivity of precipitation to regions with low wind conditions comes directly from the sensitivity of evaporation to regions with low wind conditions.

The model tends to underestimate the heaviest rain rates (see Figure 7). Figure 7 shows the daily rain rate frequency for the northern TWP region for the control and gusty simulations compared to Global Precipitation Climatology Project One Degree Daily (GPCP 1DD; Huffman et al., 2001, 2012, 2016) over the same region. The model rains too much at intermediate intensities (1–10 mm/d) and has too few

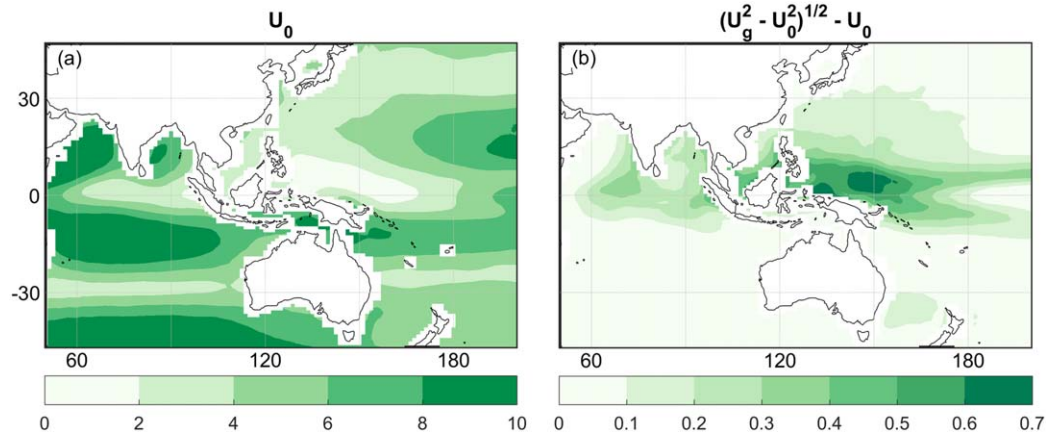


Figure 6. (a) Mean JJA resolved wind speed (m/s) in the lowest model level from the control simulation and (b) difference between gustiness wind speed and resolved wind speed based on the terms going into equations (7) and (8). Both plots are for JJA.

dry days (defined as days where the rain rate is below 0.029 mm/d). It is interesting to note that convective gustiness also increases the standard deviation of precipitation in JJA in the northern TWP (not shown). The increase in variability comes from an increase in frequency of daily precipitation with intensity exceeding 8 mm/d and a decrease in daily precipitation intensity between 0.6 and 8 mm/d compared to the control simulation (see Figure 7). It is beyond the scope of this work to explore the physical processes that give rise to the change in variability. Still, it is important to point out that gustiness does not resolve every aspect of the precipitation bias in the northern TWP region completely. While the mean bias shows large improvement, the rain rate distribution still maintains large biases. The total precipitation is coupled to the energy budget and mean overturning circulation, but the rain rate distributions are more sensitive to the model representation of convective processes and less sensitive to the inclusion convective gustiness.

Our focus is on the northern TWP region and how convective gustiness improves the summer-time precipitation bias there. The East Pacific ITCZ also shows an improvement in precipitation owing to convective gustiness (an increase in precipitation where the model has a low bias in the control). Like in the northern TWP, the increase in precipitation can be attributed to the increase in evaporation (largest term), an increase in ACRE, with the sum of those two being offset by an increase in NGMS.

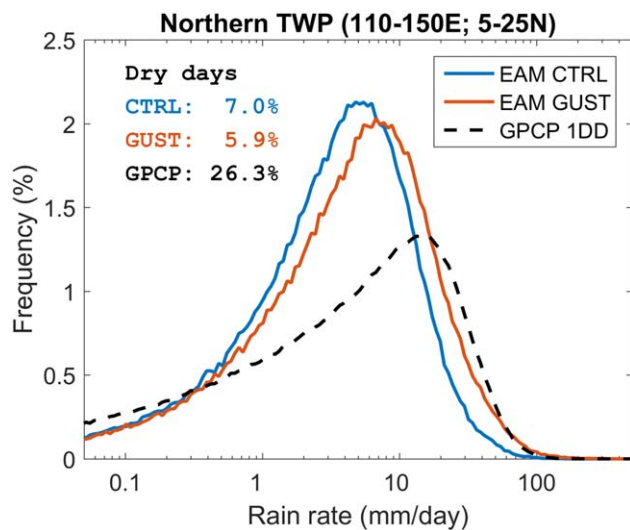


Figure 7. Rain rate frequency for control (blue solid) and gustiness (orange solid) simulations compared with GPCP 1DD data (black dashed). All data are for the northern TWP region (110–150E, 5–25N) for JJA.

3.2. Circulation Response

Where NGMS is less than one, a circulation response to forcing produces a moisture cycle response greater than that forcing. Since the increased evaporation owing to gustiness may be viewed as a positive forcing to the MSE budget, the atmospheric response may be viewed as a means of diverging additional MSE through convective processes, which naturally enhance local precipitation. Figure 5 shows gustiness increases MSE throughout the entire column north of the equator, while simultaneously enhancing both low level MSE convergence and upper level MSE divergence. The longitude range in Figure 5 is 110–150E.

It is important to recall that the predicted precipitation in Figure 2d does not account for any feedbacks or other adjustments made by the atmosphere as it moves into a new equilibrium. Therefore, we cannot expect the predicted ΔP to match the actual ΔP shown in Figure 2c. We do, however, expect the predicted ΔP to highlight regions where convective gustiness has the largest impact on precipitation, which it does. As we noted above, the circulation adjusts to export more MSE in the presence of convective gustiness. Equation (11) cannot account for these circulation changes and how the new wind field, and hence new evaporation field, will compare to the predicted

gustiness winds from the new convective precipitation field. The interplay of the circulation and precipitation sets up a feedback loop where the two continue to evolve until a new equilibrium is reached. The diagnosed ΔP shown in Figure 2e bears a much closer resemblance to the actual ΔP in Figure 2c because the evaporation field used in Figure 2e takes these feedbacks into consideration. Even then, Figures 2c and 2e are not in perfect agreement, suggesting the few small scale differences there are not captured in our diagnostic framework.

There may be land regions, such as the Amazon where precipitation is underestimated (not shown), that may benefit from including convective gustiness over both land and ocean as they fit the criteria of having both convection and weak resolved surface winds (we plan to examine the potential of the gustiness parameterization for improving the Amazon precipitation bias in future work).

3.3. Monsoon Response

While we have focused on JJA for the above analyses, it is worth stepping back to note that the northern TWP region has a strong seasonality of precipitation, with a monsoon-like distribution peaking in local summer. There are a number of available metrics for quantifying the fidelity of monsoon precipitation. One such metric is the difference between summer and winter precipitation (JJAS-DJFM) which is the dominant annual mode of variability for monsoon systems (Wang & Ding, 2008). The observed difference in JJAS-DJFM precipitation for the northern TWP region (defined here as 5–25N, 110–150E) is estimated by GPCP as 3.7 mm/d and by CMAP as 5.8 mm/d. In the control simulation, JJAS-DJFM precipitation for the same region is -0.6 mm/d, while in the experiment including convective gustiness that difference jumps up to 2.3 mm/d. A similar metric that accounts for the magnitude of the annual precipitation is the Monsoon Precipitation Index (MPI; Wang & Ding 2008). The MPI is defined as

$$\text{MPI} = \frac{\text{MJJAS} - \text{NDJFM}}{\text{Annual mean}} \quad (12)$$

For the northern TWP region, MPI estimated by GPCP is 0.61, estimated by CMAP is 0.74, in the control simulation is -0.04 , and in the gustiness experiment is 0.33. For both the simple JJAS-DJFM metric and the MPI, the control simulation dramatically under-predicts the seasonal cycle of precipitation. While including convective gustiness shows a major improvement, the seasonality is still weak compared to both observational data sets.

4. Conclusions

We have shown that convective gustiness is capable of increasing precipitation north of the maritime continent—the northern TWP region. This precipitation increase occurs because the northern TWP is a region with both convection and low climatological resolved surface winds, making it sensitive to increased evaporation from convective gustiness. These results point to low evaporation being responsible for the underestimate of precipitation in the northern TWP. While observed evaporative fluxes carry large uncertainties, the evaporation in the northern TWP region in the control simulation is less than that estimated by the Woods Hole Oceanographic Institute Objectively Analyzed Air-sea fluxes Project (Yu et al., 2008; not shown). Our results suggest that correcting this underestimate in evaporation is important for accurately simulating the Boreal summer precipitation pattern in the northern TWP.

The increase in evaporation owing to convective gustiness may be interpreted as an energy forcing to the atmosphere within a Normalized Gross Moist Stability framework, which produces an increase in precipitation. The NGMS framework correctly identifies regions such as the northern TWP where precipitation increases should be sensitive to convective gustiness. This work also highlights the importance of properly simulating the surface fluxes of heat and moisture and the continued need for observations to constrain the flow of energy through the atmosphere.

While the increase in evaporation improves the mean precipitation, biases remain in the rain rate distribution, suggesting additional work will be needed to fully rectify the precipitation biases present in the northern TWP. Additionally, the inclusion of convective gustiness changes the TOA radiation balance, which will require retuning of the model. While it is expected that tuning will alter the magnitude of the precipitation

response to gustiness, the physical processes by which evaporation acts to enhance precipitation should remain consistent with the results presented in this work.

While our work focused on the northern TWP, our analysis also suggests the Amazon region should exhibit similar sensitivities to processes like gustiness. The Amazon region, much like the northern TWP, is a region of weak large-scale winds (see Figure 6) and convective precipitation dominates the total surface precipitation flux (Figure 1). We did not, however, include gustiness over land as it is not expected to have a strong influence over the northern TWP which is mostly open ocean, and is therefore beyond the scope of this work. A thorough analysis of the role of gustiness for the Amazon basin is left to future work.

Acknowledgments

The global ocean heat flux and evaporation products were provided by the WHOI OaFlux project (<http://oafux.whoi.edu>) funded by the NOAA Climate Observations and Monitoring (COM) program. The GPCP SG combined precipitation data were developed and computed at the NASA/Goddard Space Flight Center's Mesoscale Atmospheric Processes Laboratory-Atmospheres as a contribution to the GEWEX Global Precipitation Climatology Project. The model output used in this study can be obtained at http://portal.nersc.gov/archive/home/b/beharrp/www/e3sm_gustiness_data/, and the scripts and data necessary to generate the figures are archived at <https://doi.org/10.5281/zenodo.1188987>. The authors thank our anonymous reviewers for their helpful comments and suggestions. The authors also thank Ruby Leung for useful discussion and suggestions. This research was supported as part of the Energy Exascale Earth System Model (E3SM) project, funded by the U.S. Department of Energy, Office of Science, Office of Biological and Environmental Research. We acknowledge the use of computational resources of the National Energy Research Scientific Computing Center, a DOE Office of Science User Facility supported by the Office of Science of the U.S. Department of Energy under contract DE-AC02-05CH11231. The Pacific Northwest National Laboratory is operated for the Department of Energy by Battelle Memorial Institute under contract DE-AC05-76RL01830.

References

- Adler, R. F., Huffman, G. J., Chang, A., Ferraro, R., Xie, P.-P., Janowiak, J., et al. (2003). The Version-2 Global Precipitation Climatology Project (GPCP) monthly precipitation analysis (1979–present). *Journal of Hydrometeorology*, *4*, 1147–1167. [https://doi.org/10.1175/1525-7541\(2003\)004<1147:TVGPCP>2.0.CO;2](https://doi.org/10.1175/1525-7541(2003)004<1147:TVGPCP>2.0.CO;2)
- Brunke, M. A., Zeng, X., Misra, V., & Beljaars, A. (2008). Integration of a prognostic sea surface skin temperature scheme into weather and climate models. *Journal of Geophysical Research*, *113*, D21117. <https://doi.org/10.1029/2008JD010607>
- Collins, W. D., Rasch, P. J., Boville, B. A., Hack, J. J., McCaa, J. R., Williamson, D. L., et al. (2006). The formulation and atmospheric simulation of the Community Atmosphere Model Version 3 (CAM3). *Journal of Climate*, *19*, 2144–2161. <https://doi.org/10.1175/JCLI3760.1>
- Golaz, J.-C., Larson, V. E., & Cotton, W. R. (2002a). A PDF-based model for boundary layer clouds. Part I: Method and model description. *Journal of the Atmospheric Sciences*, *59*, 3540–3551. [https://doi.org/10.1175/1520-0469\(2002\)059<3540:APBMFB>2.0.CO;2](https://doi.org/10.1175/1520-0469(2002)059<3540:APBMFB>2.0.CO;2)
- Golaz, J.-C., Larson, V. E., & Cotton, W. R. (2002b). A PDF-based model for boundary layer clouds. Part II: Model results. *Journal of the Atmospheric Sciences*, *59*, 3552–3571. [https://doi.org/10.1175/1520-0469\(2002\)059<3552:APBMFB>2.0.CO;2](https://doi.org/10.1175/1520-0469(2002)059<3552:APBMFB>2.0.CO;2)
- Huffman, G. J., Adler, R. F., Morrissey, M. M., Bolvin, D. T., Curtis, S., Joyce, R., et al. (2001). Global precipitation at one-degree daily resolution from multisatellite observations. *Journal of Hydrometeorology*, *2*, 36–50. [https://doi.org/10.1175/1525-7541\(2001\)002<0036:GPAODD>2.0.CO;2](https://doi.org/10.1175/1525-7541(2001)002<0036:GPAODD>2.0.CO;2)
- Huffman, G. J., Bolvin, D. T., & Adler, R. F. (2012). *GPCP version 2.2 SG combined precipitation data set*. Asheville, NC: WDC-A, NCDC. Retrieved from <https://precip.gsfc.nasa.gov/>
- Huffman, G. J., Bolvin, D. T., & Adler, R. F. (2016). *GPCP version 1.2 one-degree daily precipitation data set*. Boulder, CO: Research Data Archive at the National Center for Atmospheric Research, Computational and Information Systems Laboratory. Retrieved from <https://doi.org/10.5065/D6D50K46>, accessed 15 November 2017.
- Jabouille, P., Redelsperger, J. L., & Lafore, J. P. (1996). Modification of surface fluxes by atmospheric convection in the TOGA COARE region. *Monthly Weather Review*, *124*, 816–837. [https://doi.org/10.1175/1520-0493\(1996\)124<0816:MOSFBA>2.0.CO;2](https://doi.org/10.1175/1520-0493(1996)124<0816:MOSFBA>2.0.CO;2)
- Larson, V. E., & Golaz, J.-C. (2005). Using probability density functions to derive consistent closure relationships among higher-order moments. *Monthly Weather Review*, *133*, 1023–1042. <https://doi.org/10.1175/MWR2902.1>
- Larson, V. E., Golaz, J., & Cotton, W. R. (2002). Small-scale and mesoscale variability in cloudy boundary layers: Joint probability density functions. *Journal of the Atmospheric Sciences*, *59*, 3519–3539. [https://doi.org/10.1175/1520-0469\(2002\)059<3519:SSAMVI>2.0.CO;2](https://doi.org/10.1175/1520-0469(2002)059<3519:SSAMVI>2.0.CO;2)
- Miller, M. J., Beljaars, A. C. M., & Palmer, T. N. (1992). The sensitivity of the ECMWF model to the parameterization of evaporation from the tropical oceans. *Journal of Climate*, *5*, 418–434. [https://doi.org/10.1175/1520-0442\(1992\)005<0418:TSOTEM>2.0.CO;2](https://doi.org/10.1175/1520-0442(1992)005<0418:TSOTEM>2.0.CO;2)
- Neale, R. B., Richter, J. H., & Jochum, M. (2008). The impact of convection on ENSO: From a delayed oscillator to a series of events. *Journal of Climate*, *21*, 5904–5924. <https://doi.org/10.1175/2008JCLI2244.1>
- Neale, R. B., Chen, C.-C., Gettelman, A., Lauritzen, P. H., Park, S., Williamson, D. L., et al. (2012). Description of the NCAR Community Atmosphere Model (CAM 5.0) (NCAR Tech. Notes Ncar/Tn-464+Str, 214 p.). Boulder, CO: National Center For Atmospheric Research.
- Raymond, D. J., Sessions, S. L., & Fuchs, Ž. (2007). A theory for the spinup of tropical depressions. *Quarterly Journal of the Royal Meteorological Society*, *1754*, 1743–1754. <https://doi.org/10.1002/qj.125>
- Raymond, D. J., Sessions, S. L., Sobel, A. H., & Fuchs, Ž. (2009). The mechanics of gross moist stability. *Journal of Advances in Modeling Earth Systems*, *1*, 9. <https://doi.org/10.3894/JAMES.2009.1.9>
- Redelsperger, J. L., Guichard, F., & Mondon, S. (2000). A parameterization of mesoscale enhancement of surface fluxes for large-scale models. *Journal of Climate*, *13*, 402–421. [https://doi.org/10.1175/1520-0442\(2000\)013<0402:APOMEO>2.0.CO;2](https://doi.org/10.1175/1520-0442(2000)013<0402:APOMEO>2.0.CO;2)
- Sperber, K. R., Annamalai, H., Kang, I.-S., Kitoh, A., Moise, A., Turner, A., et al. (2013). The Asian summer monsoon: An intercomparison of CMIP5 vs. CMIP3 simulations of the late 20th century. *Climate Dynamics*, *41*, 2711–2744. <https://doi.org/10.1007/s00382-012-1607-6>
- Wang, B., & Ding, Q. (2008). Global monsoon: Dominant mode of annual variation in the tropics. *Dynamics of Atmospheres and Oceans*, *44*, 165–183. <https://doi.org/10.1016/j.dynatmoce.2007.05.002>
- Webster, P. J., & Lukas, R. (1992). TOGA COARE: The coupled ocean—Atmosphere response experiment. *Bulletin of the American Meteorological Society*, *73*, 1377–1416. [https://doi.org/10.1175/1520-0477\(1992\)073<1377:TCTCOR>2.0.CO;2](https://doi.org/10.1175/1520-0477(1992)073<1377:TCTCOR>2.0.CO;2)
- Xie, P., & Arkin, P. A. (1996). Analyses of global monthly precipitation using gauge observations, satellite estimates, and numerical model predictions. *Journal of Climate*, *9*, 840–858. [https://doi.org/10.1175/1520-0442\(1996\)009<0840:AOGMPU>2.0.CO;2](https://doi.org/10.1175/1520-0442(1996)009<0840:AOGMPU>2.0.CO;2)
- Xie, P., & Arkin, P. A. (1997). Global precipitation: A 17-year monthly analysis based on gauge observations, satellite estimates, and numerical model outputs. *Bulletin of the American Meteorological Society*, *78*, 2539–2558. [https://doi.org/10.1175/1520-0477\(1997\)078<2539:GPAYMA>2.0.CO;2](https://doi.org/10.1175/1520-0477(1997)078<2539:GPAYMA>2.0.CO;2)
- Yu, L., Jin, X., & Weller, R. A. (2008). *Multidecade global flux datasets from the Objectively Analyzed Air-sea Fluxes (OaFlux) Project: Latent and sensible heat fluxes, ocean evaporation, and related surface meteorological variables* (Oa-2008-01, 64 p.). Woods Hole, MA: Woods Hole Oceanographic Institution. <https://doi.org/10.1007/s00382-011-1115-0>
- Zeng, X. B., Zhang, Q., Johnson, D., & Tao, W. K. (2002). Parameterization of wind gustiness for the computation of ocean surface fluxes at different spatial scales. *Monthly Weather Review*, *130*, 2125–2133. [https://doi.org/10.1175/1520-0493\(2002\)130<2125:POWGGT>2.0.CO;2](https://doi.org/10.1175/1520-0493(2002)130<2125:POWGGT>2.0.CO;2)
- Zhang, G. J., & McFarlane, N. A. (1995). Sensitivity of climate simulations to the parameterization of cumulus convection in the Canadian climate centre general circulation model. *Atmosphere-Ocean*, *33*, 407–446. <https://doi.org/10.1080/07055900.1995.9649539>